Eccentric Birth Rings and Asymmetric Debris Disks

Joseph M. Hahn
Space Science Institute
Austin, TX

Introduction

Debris disks are the dusty circumstellar disks that are known to orbit a number of nearby stars. These dust disks are transient and must also be replenished, since collisions as well as stellar radiation forces tend to drain a disk of its dust. These disks are thought to be replenished by an unseen 'birth ring' of planetesimals whose collisions generate the observed dust. Small dust can then drift inwards of the ring due to Poynting-Robertson drag, with even smaller dust grains being lofted outwards into wide orbits (~ 100's of AU) by radiation pressure (Strubbe & Chiang 2006). These two different transport mechanisms also cause the dust-disk's optical depth to change at the birth-ring's radius a_r. And when such a disk is viewed edge on, as for AU Mic and β Pic, this also causes the disk's surface brightness to fall of rapidly as $\propto r^{-3.5}$ at projected distances of $r \gg a_r$, and less rapidly at $r \ll a_r$ (Strubbe & Chiang 2006); see also Fig. 1.

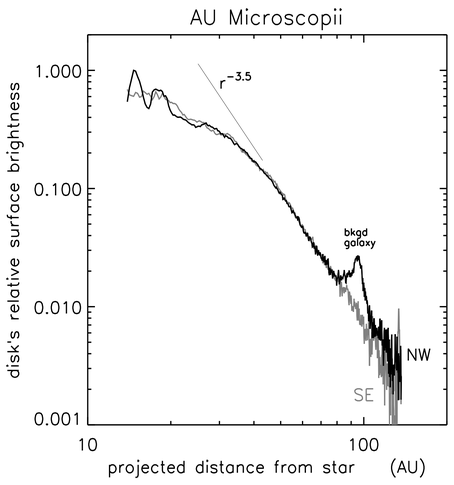

FIGURE 1: Surface brightness profiles of the AU Mic debris disk, plotted versus projected distance from the central star, along its northwest (NW) and southeast (SE) ansae. These profiles are extracted from an optical HST image provided by John Krist and described in Krist et al (2005). Note that the outer disk's profile varies as $r^{-3.5}$ at $r \gg 43$ AU, while its inner profile has a shallower slope. This is the signature of a birth ring of planetesimals orbiting at $a_r \simeq 43$ AU (Strubbe & Chiang 2006). Although it is hard to see in this figure, the NW ansa is $\sim 2\times$ brighter than the SE ansa at distances of $r \gtrsim 100$ AU (Krist et al 2005).

These dust-disks are often asymmetric. For instance, the northwest ansa of the AU Mic debris disk is ~ 2 brighter than the southeast ansa at projected distances of $r \gtrsim 100$ AU (Krist et al 2005), the while NE ansa of the β Pic disk is $\sim 50\%$ brighter than its SW half beyond $r \gtrsim 200$ AU (from HST observations provided by David Golimowski). This asymmetry is also quite evident in the recent image of HD 32297 (see Fig. 2).

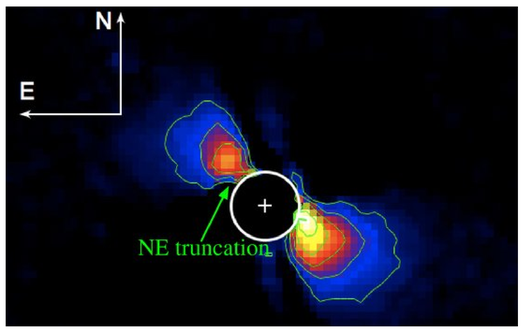

FIGURE 2: HST NICMOS observations of the debris disk orbiting HD 32297, from Debes at al (2009).

We suspect that the large-scale asymmetries that are routinely seen in these debris disks are due to the birth ring's eccentricity. Note that when the birth ring is eccentric, the dust size-threshold for blow-out via radiation pressure becomes sensitive to the longitude in the ring where the dust is generated. As the following shows, this will cause one side of the disk to be overdense with the smaller grains that tend to dominate a disk's optical depth, which gives the disk a 'lopsided' appearance.

Dust orbits

An orbiting dust grain is characterized by its dimensionless size parameter $\beta = 3L_\star/16\pi GM_\star \rho R c$, which is the ratio of radiation pressure to stellar gravity, and all symbols have their usual meaning, so grains with smaller radii R have larger β.

A dust grain is produced by a collision among planetesimals in the birth ring. The just-formed dust grain will have the same velocity as its parent planetesimal, but behaves as if orbiting a star whose mass is reduced by a factor $1-\beta$ due to radiation pressure, which injects the grain into a wide, eccentricic orbit. With this in mind, it is straightforward to derive the dust grain's semimajor axis a, eccentricity e, and longitude of peripase $\tilde{\omega}$, all as functions of the grain size parameter β:

$$a = \frac{(1-\beta)a_r}{1-2\beta a_r/r_r}, \qquad e = \sqrt{1-\frac{a_r}{a}\left(\frac{1-e_r^2}{1-\beta}\right)}, \quad \text{and} \quad \tan\tilde{\omega} = \frac{\beta\sin\theta_r}{\beta\cos\theta_r + e_r} \quad (1)$$

where a_r and e_r are the birth-ring's orbit elements, and (r_r, θ_r) are the polar coordinates in the ring where the grain is formed.

Figure 3 illustrates the range of trajectories that result for grains having a variety of sizes β. For instance, dust having $\beta < (1-e_r)/2$ can be launched from all longitudes within the birth ring and still stay bound to the system such that $a > 0$; see upper Fig. 3. Note also that trajectories tend to be elongated towards the birth-ring's apoapse, *ie* towards the left side in Fig. 3. This is due to the dust grains' higher velocities when launched from the birth-ring's periapse (right side of Fig. 3).

Smaller dust grains having even larger β can only stay bound to the star when launched at longitudes nearer the ring's longitude of apoapse. This is due to the birth-ring's lower orbital velocity there; see insets to Fig. 3. Smaller dust grains also travel out to greater distances from the central star, while larger dust grains are confined nearer the birth ring. Also note that all dust having $\beta > (1+e_r)/2$ have $a < 0$, are not bound, and quickly leave the system.

Lastly, note that all of the patterns seen here are non-axisymmetric; many of the trajectories tend to be elongated towards the birth-ring's apoapse (to the left of Fig. 3), while the dust streamlines tend to be most dense towards the ring's periapse (to the right). Also it is the latter effect that tends to make the circumstellar debris disk overdense and thus brighter in the direction of the birth ring's periapse.

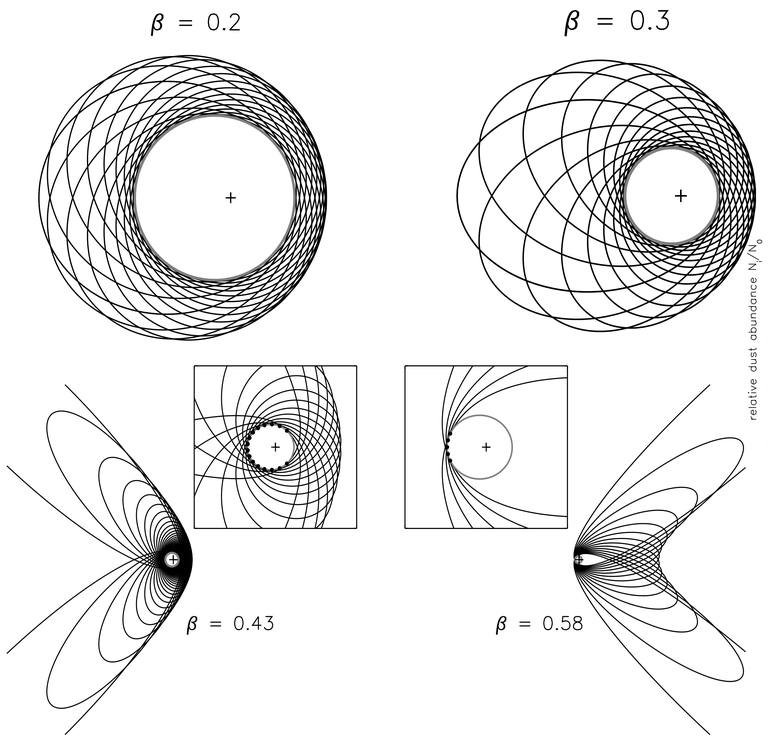

FIGURE 3: Dust trajectories for grains of size β launched at discrete longitudes withing an eccentric birth ring. The birth ring has eccentricity $e_r = 0.2$, and is indicated by the grey ellipse whose size also provides the spatial scale for each figure. A cross denotes the central star. Dust having sizes $0.4 < \beta < 0.6$ are only bound to the system when launched from longitudes nearer the ring's apoapse (to the left in each figure), due to the parent body's lower velocity there. This is indicated in the inset figures that zoom in on the birth ring, which uses dots to indicate those longitudes in the ring that can generate bound dust.

Assuming the dust in a disk have some power-law size distribution, $dN/dR \propto R^{-q}$, then one can easily estimate the dust disk's optical depth $\tau(r)$ versus distance r (see left Fig. 4), which shows that the disk is indeed more dense in the direction of periapse. This simulated disk is then viewed edge-on, along a line-of-sight that is perpendicular to the birth ring's long axis. Surface brightness profiles are then computed (see Fig. 4, right), which shows that the periapse side of the disk is indeed brighter than the apoapse side.

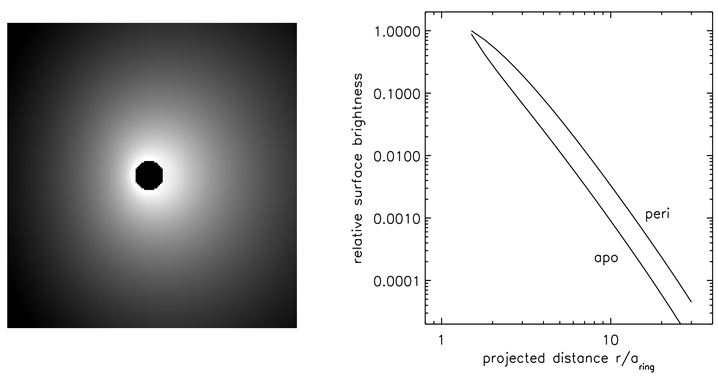

FIGURE 4: *Left:* Surface brightness map of a model debris disk seen via reflected starlight. This disk is generated by a birth ring having eccentricity $e_r = 0.2$ and a very steep dust size distribution $q = 8$. The greyscale shows that the resulting disk is lopsided and brighter in the direction of the ring's periapse, which is to the right. *Right:* Surface brightness profiles of this disk as it is viewed edge-on, with the LOS running bottom to top. The ansa in the direction of the ring's periapse is ~ 3.5 times brighter than the apoapse side.

Dust collisions

However, the cartoon model described above does not account for collisions among dust grains, which tends to deplete the disk over time. Collisions are also important here, because the smaller dust grains are longer lived, which steepens the dust size distribution. And because it is the smallest grains whose orbits show the most asymmetry (see Fig. 3), collisions will also magnify the disk's asymmetry.

To account for collisions, first *quantize* the problem, and assume that the birthring is the source of numerous discreet dusty streamlines (or orbits) in the disk, each characterized by a grain size β and orbits $a(\beta), e(\beta), \tilde{\omega}(\beta)$. This quantization allows one to avoid slow Monte Carlo simulations as well as really slow Nbody simulations, and also replaces tedious 3D integrals over the disk volume with sums. The model then inspects every site where pairs of streamlines cross, and calculates a collision probability density α_{ij}. This then provides rate equation for the dust abundance $N_i(t)$ in each streamline i:

$$\frac{dN_i}{dt} = \text{dust production} - \text{collisional destruction rates} = p_i - N_i \sum_{j \neq i} \alpha_{ij} N_j$$

where the dust production rate p_i is a power law in the grain radiii R_i. This coupled system of equations is easily solved for the streamline populations $N_i(t)$, which in turn provides the disk's optical depth $\tau(r)$ and surface brightness $B(\ell)$ versus projected distance ℓ from the star; see Fig. 5.

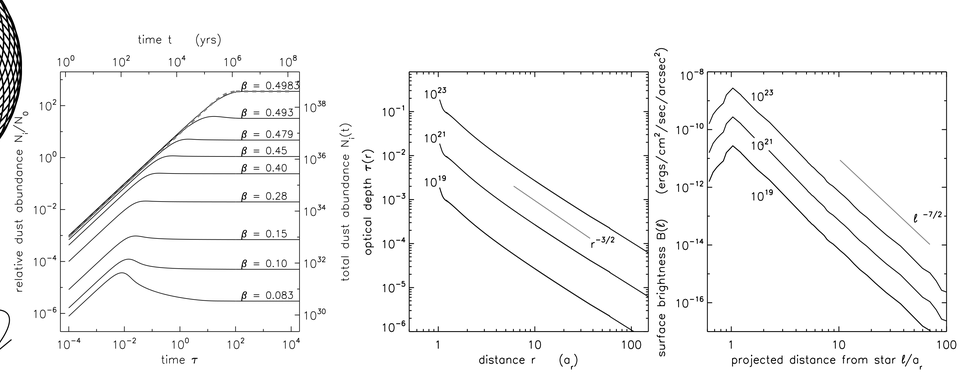

FIGURE 5: *Left:* Number of dust grains $N(\beta_i, t)$ for the for dust of size β_i versus time t for a debris disk generation by a birth ring whose dust production rate is $\dot{M}_d = 10^{23}$ gm/yr with a $q = 4$ differential size distribution. *Middle:* the disk's optical depth $\tau(r)$ for birth ring's having various dust production rates $\dot{M}_d$ in units of gm/yr. *Right:* The edge-on debris disk's surface brightness $B(\ell)$ versus projected distance ℓ from the star.

Results thus far

As Fig. 5 shows, the debris disk's optical depth $\tau(r)$ and surface brightness $B(\ell)$ are both quite sensitive to the birth ring's dust production rate $\dot{M}_d$, with both varying as $\sqrt{\dot{M}_d}$. So by comparing these simulations to the surface brightness of the observed disks orbiting β Pic, AU Mic, HD 32297, and others, we should be able to extract dust production rates for those systems, as well as the total mass of dust in the disk. Matching the simulated to observed asymmetries will also provide measurements of the unseen birth ring's eccentricity e_r. Those results will be in hand in the coming weeks.

Acknowledgments:

Support for this work was provided by NASA via a Hubble Theory/Archive grant from the Space Telescope Science Institute.

References

Chiang, Kite, Kalas, Graham, Clampins, 2009, ApJ, 693, 734.
Goldstein, 1980, in Classical Mechanics.
Debes, Weinberger, Kuchner, 2009, ApJ, 702, 318.
Golimowski, 42 coauthors, 2006, AJ, 131, 3109.
Krist, 40 coauthors, 2005, AJ, 129, 1008.
Strubbe, Chiang, 2006, ApJ, 648, 652.